Biomedical Signal Processing and Control 86 (2023) 105071

Contents lists available at ScienceDirect

Biomedical Signal Processing and Control

journal homepage: www.elsevier.com/locate/bspc

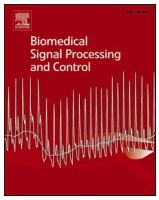

Classification of pulmonary arterial pressure using photoplethysmography and bi-directional LSTM

Qian Zhang , Pei Ma *

Key Laboratory of Optical Technology and Instrument for Medicine, Ministry of Education, College of Optical Electrical and Computer Engineering, University of Shanghai for Science and Technology, Shanghai 200093, China

A R T I C L E I N F O

Keywords:
Photoplethysmography
Pulmonary hypertension
Wavelet scattering

A B S T R A C T

Pulmonary hypertension (PH) is an obstructive progressive disease of lung vascular system which is usually associated with congenital heart disease (CHD) and it induces the right ventricle failure, adversely affecting quality of life and survival. Pulmonary arterial pressure (PAP) is a direct indicator of PH. The existing PAP measurement techniques are invasive and inconvenient, which are not suitable for frequent use or long time monitoring. A noninvasive and convenient method for measuring PAP is essential for the early prevention and diagnosis of PH. The aim of this study was to propose and evaluate a deep learning approach for the classification and evaluation of pH from noninvasive photoplethysmography (PPG) signals. A wavelet scattering transform method was used to automatically extract features from PPG signals. Then a Bi-directional long short-term memory network (Bi-LSTM) was developed to learn extracted features and finally output the predicted PAP classification results. Based on the results from 216 patients' records, a classification accuracy of 98.52% was presented. This indicated that the Bi-LSTM model trained on features extracted from PPG signals has satisfying performance in PAP classification. This method will enable the noninvasive and painless measurement of PAP. With the development of wearable devices to capture PPG signals from fingertips and the emergence of deep learning models, noninvasive and convenient PAP predictions will greatly contribute to the early diagnosis and prevention of cardiovascular diseases.

1. Introduction

Pulmonary arterial pressure (PAP) refers to the lateral pressure generated by blood flowing through pulmonary circulation on pulmonary artery vessels, and it is an important indicator of clinical hemodynamics [1]. PAP is different from blood pressure. Blood pressure is an indicator of systemic circulation pressure, while PAP is an indicator of pulmonary circulation pressure. It includes pulmonary artery systolic pressure and diastolic pressure, which reflects right ventricular systolic function and pulmonary artery vascular resistance, respectively [2]. Mean pulmonary artery pressure refers to the mean pulmonary artery pressure during a complete systolic and diastolic period and is often used to assess the mean pressure experienced by the pulmonary arterial system. As an indicator of right ventricular after-load, PAP represents the resistance that the right ventricle must overcome when pumping blood. Elevated PAP leads to the increase of the load of the right ventricle, then to right ventricular hypertrophy, and ultimately to right heart failure [3]. According to National Institutes of Health (NIH), the mean untargeted survival time after diagnosis of idiopathic pulmonary hypertension(PH) was 2.8 years [4].

As PH is gradually aggravated, it is important to monitor PAP in high-risk population, yet it is not easy. Patients with PH usually show early symptoms of difficulty in breathing, fatigue, and chest pain, which are common symptoms that occur in many other diseases, such as pulmonary infection and hypothyroidism [5]. Also, the gold standard measurement for PAP, right ventricular catheterization (RHC), is an invasive and complex procedure [6]. In RHC, a right heart catheter is inserted through a vein to the right heart chamber and great vessels under the guidance of X-ray fluoroscopy [7]. Apparently, RHC gives pain to patients and it is difficult to be performed frequently for the assessment of disease progression or treatment responses. In addition, RHC has the potential to increase the risk of heart disease in patients undergoing non-cardiac surgery [8]. Researchers have been trying to develop noninvasive alternatives for estimating PAP. For example,

* Corresponding author at: Key Laboratory of Optical Technology and Instrument for Medicine, Ministry of Education, College of Optical Electrical and Computer Engineering, University of Shanghai for Science and Technology, Shanghai 200093, China.
E-mail address: peima@usst.edu.cn (P. Ma).

https://doi.org/10.1016/j.bspc.2023.105071
Received 27 November 2022; Received in revised form 15 April 2023; Accepted 23 May 2023
Available online 9 June 2023

echocardiography has been used to diagnose pulmonary hypertension [9,10]. However, concerns remain regarding the accuracy of echocardiographic measurements of PAP [11]. Noninvasive and convenient methods for measuring or predicting PAP is still in urgent need for the early diagnosis of pH and for monitoring the disease progression.

We have noticed the potential of photoplethysmography (PPG) in providing indications of PH. PPG signal is a complex mixture that comes from the blood flow in arteries and veins of the cardiovascular circulatory system, and is therefore used in monitoring a variety of physiological parameters, especially cardiovascular parameters [12-14]. PPG is a measurement on the skin surface in a non-invasive way, by emitting green light (500–560 nm) or low intensity infrared light to the tissue, and collecting the transmitted or reflected light with a photoelectric receiver [15]. When the heart periodically beats, PPG measures the periodic changes in the light absorption of the blood, and gives a profile of blood volume changes over time [16]. PPG was used in the prediction of blood pressure, hypertrophic cardiomyopathy, coronary artery disease, cardiac output and respiration [17-20].

PPG measurement is also low-cost and convenient. Especially, the recent development of deep learning methods has improved the classification and prediction accuracy of using PPG in disease diagnosis [18]. Ward et al. tested a deep learning method for the classification and evaluation of normal blood pressure and hypertension using PPG signals based on the continuous wavelet transform and pretrained convolutional neural network, and reached a 92.55% accuracy [21]. Lin et al. used radial blood pressure waveform and PPG Pulse Indices as features of multilayer perceptron (MLP) analysis method, which could distinguish mild, moderate and severe Alzheimer's disease with an accuracy of about 82.86% [22].

Radha et al. achieved classification of 4-class sleep stage based on PPG signal and transfer learning model. The model structure consists of domain layer, temporal layer and decision layer. Among them, temporal layer consists of the LSTM stacks, decision layer consists of two levels of perceptions. The model exhibits good performance with an accuracy of 76.36 ± 7.57% [23].

In this paper, a novel method for pulmonary arterial pressure (PAP) classification using wavelet scattering transform feature extraction module combined with a bidirectional long short-term memory (Bi-LSTM) network was proposed. It only requires PPG signals collected from a single fingertip site as the input, and avoids measuring PAP invasively. The output of the model is the classification of PAP, including normal pulmonary arterial pressure (NPP), early pulmonary hypertension (EPH), and pulmonary hypertension (PH). The identification and classification of PAP were achieved with the following steps (Fig. 1): 1. screening, extraction and preprocessing of PPG signals; 2. apply wavelet scattering transform technique to extract signal features; 3. train a Bi-LSTM network model; 4. classification of different PAP stages. The method was evaluated with database that contains gold-standard RHC measurements and the test accuracy was above 96%. This method used PPG signals to achieve the classification and diagnosis of PH, providing a non-invasive alternative in determining the risk in PAP. If further combined with wearable devices, convenient, frequent and long-term PAP monitoring will be enabled. Thus, the pain and risk of patients would be significantly reduced.

2. Materials, algorithms and methods

2.1. Dataset

This study collected a subset of 250 records from the Multiparameter Intelligent Monitoring (MIMIC) II online database provided by the PhysioNet organization [24]. The MIMIC-II database is a freely available, de-identified database containing high-resolution time series of physiological signals and vital signs of adult patients treated in the Intensive Care Unit (ICU) [25]. Each record includes arterial blood pressure, electrocardiogram, PPG, PAP, etc. Typically, these signals were sampled at 125 Hz with 8 or 10-bit precision. In the collected dataset, each recording contained both PPG and PAP signals acquired simultaneously from a patient. The PAP signal was recorded invasively with RHC method and the PPG signal was recorded from the fingertip.

The PAP level label used in the training of the model was extracted from the PAP signal. According to the World Symposium on Pulmonary Hypertension (WSPH) standard, PAP levels were classified as normal pulmonary arterial pressure (NPP), mild, moderate, and severe pulmonary hypertension. Because both moderate and severe pulmonary hypertension present obvious symptoms of dyspnea, they can be put into the same category as pulmonary hypertension [5]. Therefore, in this study, the PAP levels labels were NPP, EPH and PH.

The PPG signals went through pre-processing and feature extraction before entering the Bi-LSTM model. Fig. 2 showed the waveforms of the two types of signals and how were they used in the model.

2.2. Signal pre-processing

The raw PPG data was pre-processed before fed into the Bi-LSTM model. The waveforms generally contain baseline drift, varying degrees of distortion and irregular segments affected by motion, and non-anomalous segments. Therefore, several pre-processing steps were performed in order to maximize the useful information in the original PPG signals.

First, incorrect and flawed PPG fragments were screened out. Fig. 3 showed examples of appropriate and excluded unsuitable PPG fragments. Then, we used MATLAB (version 2021b) to perform filtering with a 0.5–12 Hz, fourth-order Butterworth bandpass filter. This was used to filter out interference and noise, and remove low frequency baseline drift of PPG. Finally, the amplitude of each PPG signal was normalized to [0, 1] using min–max normalization. Fig. 4 showed the comparison of the PPG signal before and after preprocessing.

2.3. Feature extraction

In order to establish a reliable and efficient PAP classification model, feature extraction of PPG signals was performed before inputting the signals into the neural network. In this study, a signal analysis method

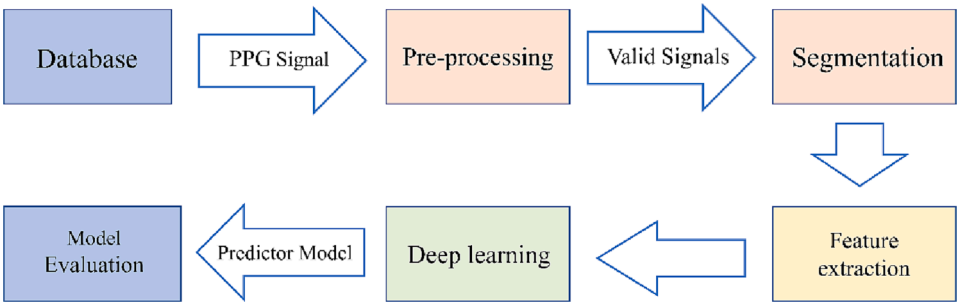

Fig. 1. System workflow of the method.

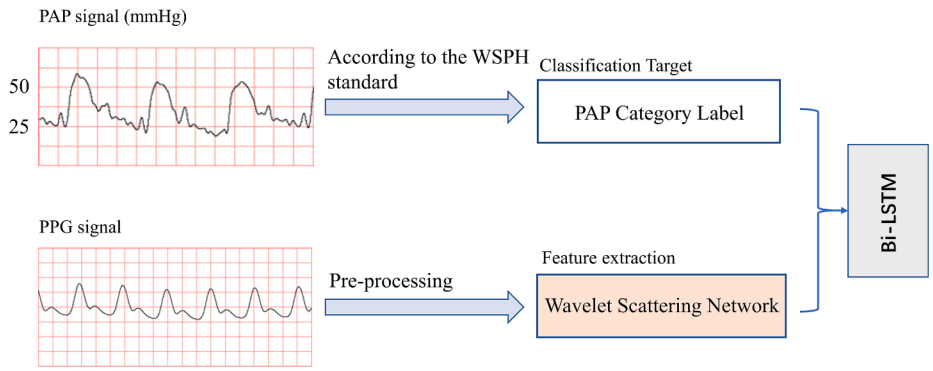

Fig. 2. Waveform and purpose of the two signals.

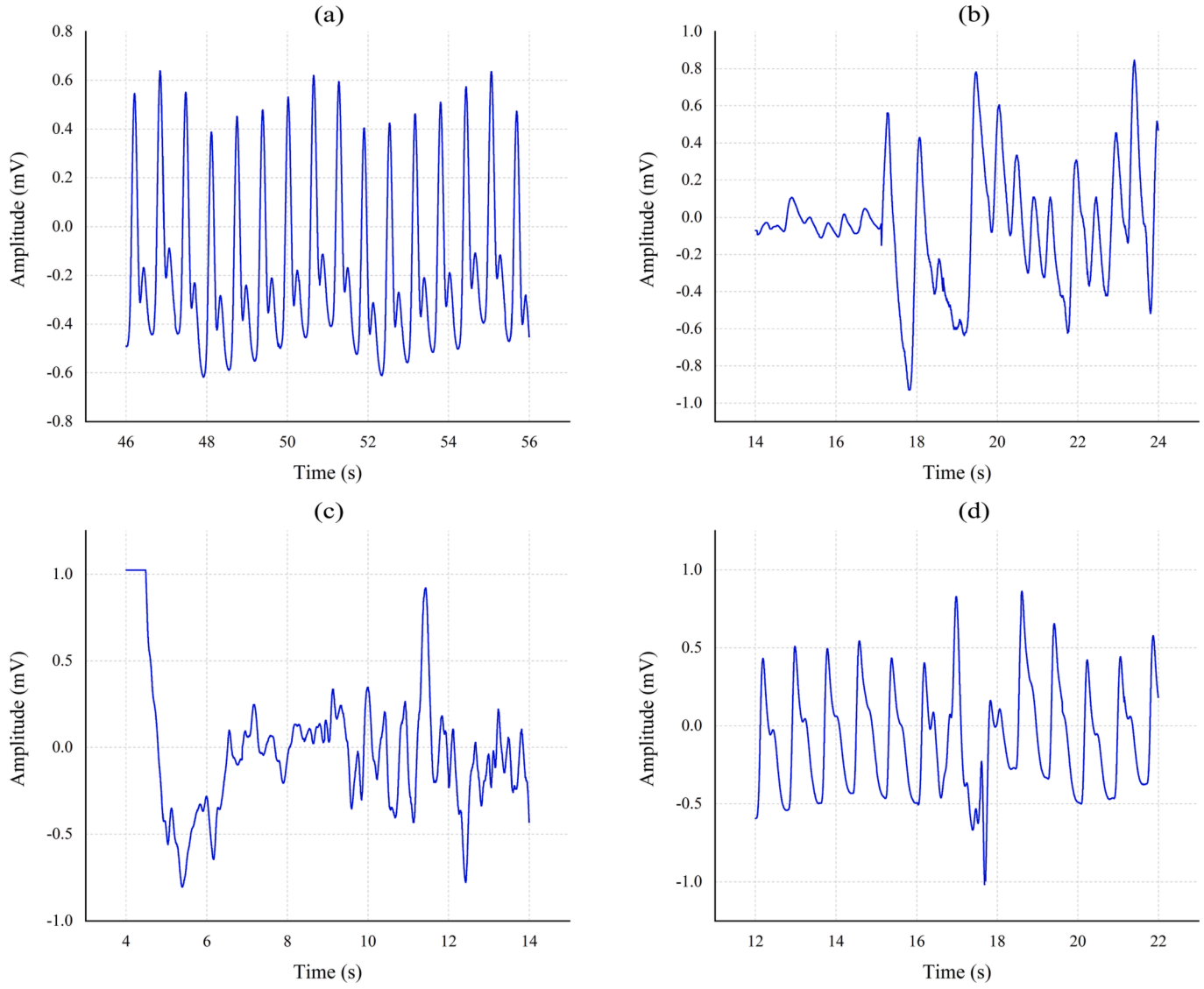

Fig. 3. Example of (a) appropriate PPG segments. (b)(c) and (d) inappropriate PPG segments.

called wavelet scattering transform was used to extract features from PPG signals. Wavelets scattering transform refers to the oscillatory waveform of the mother wavelet with finite length or fast decay to represent the signal. The waveform is scaled and shifted to best fit the signal, stretching wavelets help capture changes that occur slowly in the signal, and compressing wavelets help capture mutations. A new signal representation is created with a linear combination of wavelets. In the process of representing the signal as a series of linear combinations of wavelet functions with different scales and different time shifts, the coefficients of each term are called wavelet coefficients, which show the similarity between the wavelet and the signal.

The wavelet scattering transform method can extract local

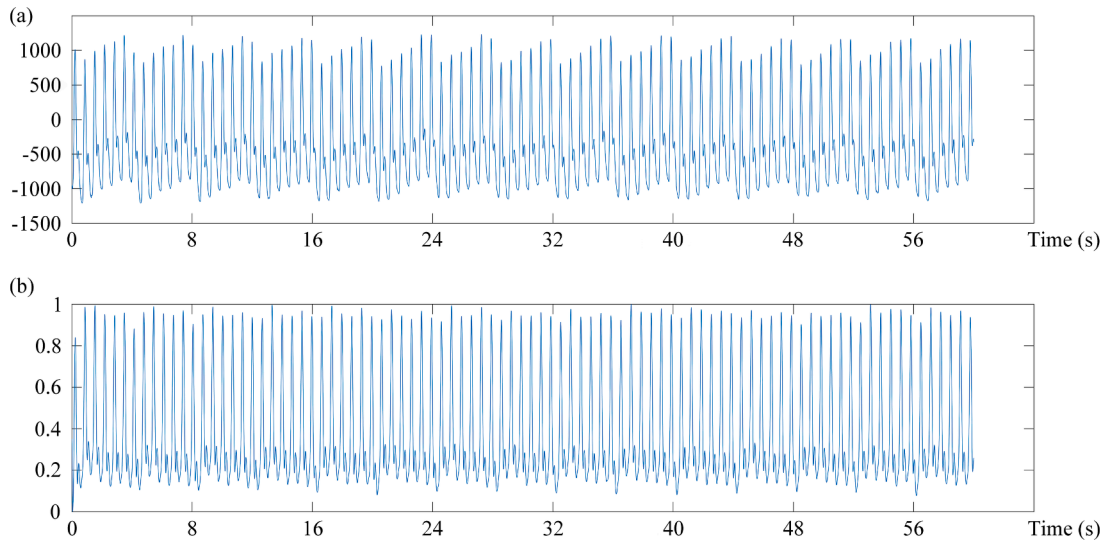

Fig. 4. PPG signal before (a) and after (b) pre-processing.

time–frequency features of signals, and has good adaptability to different frequency components and time-domain structural features of one-dimensional signals [26,27]. It has good time and frequency resolution and can be used extract more comprehensive and accurate features [28]. All of these advantages were especially useful in the feature extraction of PPG signals, because it is a kind of 1D time sequence and its waveform contains a large number of features.

Wavelet scattering transform was realized by the wavelet scattering transform network, also known as invariant scattering convolutional network, which is a framework for automatic feature extraction [29]. Each layer consists of three parts: convolution, nonlinearity and averaging. Among them, convolution is performed by wavelet, and modulus operator was used for nonlinearity. Its structure was shown in Fig. 5. The original PPG signal F was equally divided into time windows f1, f2, f3…, fn. The processing of each time window was identical. Using f1 as an example, the feature extraction was described and the flowchart was shown in Fig. 6. First, use the scale filter Φ, a low-pass filter, to perform an average operation on f1 to obtain average signals, which was represented by f1*Φ, the result of the 0th layer. However, the high-frequency details in the signal were lost in the averaging. In order to capture the high-frequency details, a wavelet filter Ψ, which was a high-pass filter, was applied to the original signal f1 to acquire f1*Ψ. High pass filtering preserved the details of the signal and recovers the detailed information lost during low pass filtering. The modulus of the high pass filtered output was taken (|f1*Ψ|), and was then filtered with the low pass filter Φ to obtain |f1*Ψ|*Φ. Similarly, the output of the high pass filter is|f1*Ψ|*Ψ and the modulus is||f1*Ψ|*Ψ|, and the result of the second layer of low pass filter was ||f1*Ψ|*Ψ|* Φ. That is, the high-pass filtered output of the previous layer will become the input to the operation of the next layer, then the same modulus operator is applied, and a wavelet low pass function is applied for filtering. The output of the low pass filtering produces scattering coefficients that represent the signal at each layer, and these coefficients are called scattering features. Select the next time window and repeat the process above for f2 and f3…, fn. The operation of extracting wavelet scattering transform features was completed in MATLAB (version 2021b). Table 1 showed the comparison before and after wavelet scattering transform processing with two filterbanks, from 3750 samples to 1592 samples.

2.4. Bi-LSTM model

PPG features acquired in the previous step were used as the input of the Bi-LSTM network for the classification of PAP. Bi-LSTM is derived from the long short-term memory (LSTM) network. LSTM is a special recurrent neural network (RNN) [30]. Generally, RNN faces problems of gradient disappearance and gradient explosion when learning long sequences [31]. LSTM was designed to solve this problem by improved internal structure [32]. The LSTM network has obvious advantages in 1D signal classification. It is able to capture the time dependence and long-term dependence in the data [33]. At the same time, the gating mechanism of LSTM can effectively prevent gradient vanishing and improve the training efficiency and accuracy of the model [27].

There are three stages inside LSTM: forget gate, which filters the input (output of the previous node) to exclude unimportant information;

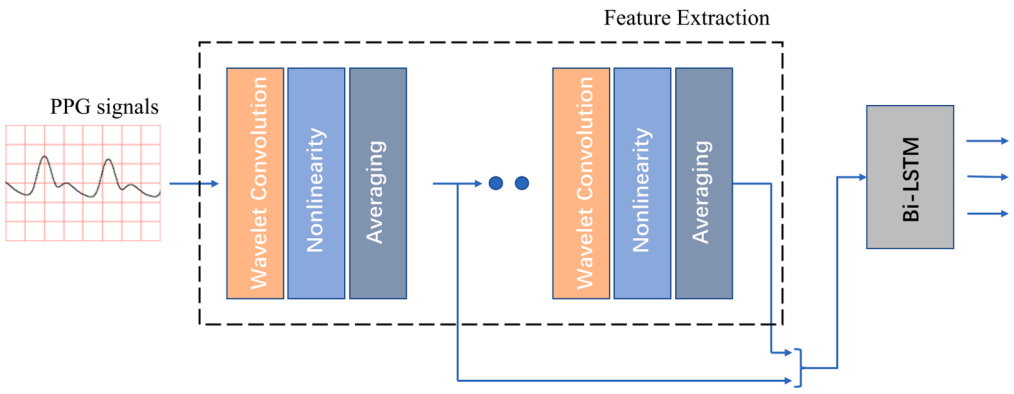

Fig. 5. Structure of wavelet scattering transform network.

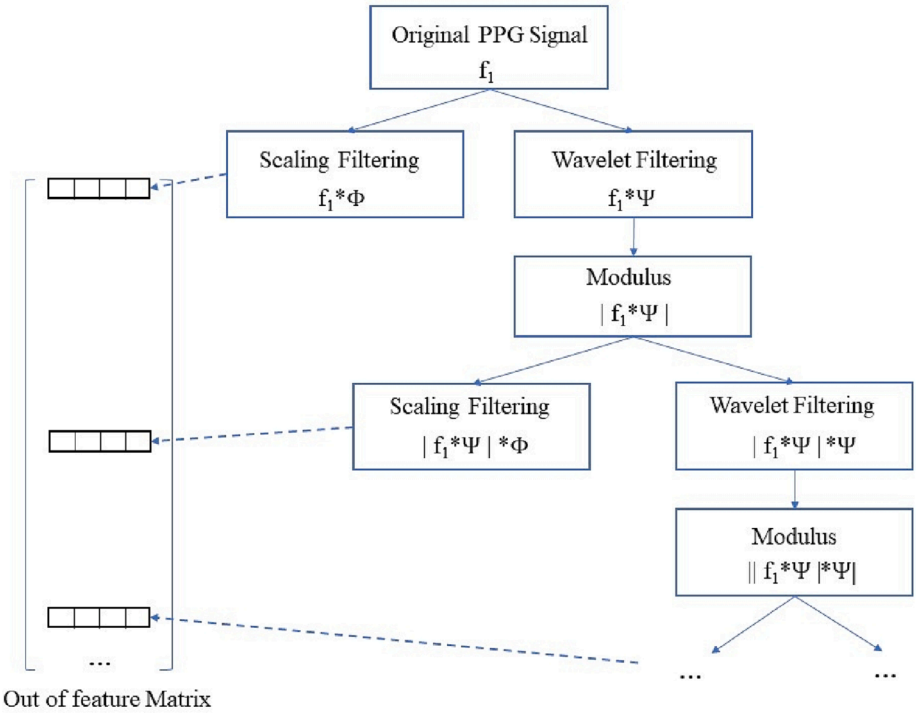

Fig. 6. Flowchart of extracting wavelet scattering transform features.

Table 1
Comparison before and after wavelet scattering transform processing.

Name	Size	Bytes	Class
Input signals	1 × 3750	30,000	double
Feature	199 × 8	12,736	double

input gate, which focuses on memorizing the important information of the input X(t), the PPG signal after feature extraction; output gate, which decides the final classification as the output. The input X(t) and the h(t-1) passed from the previous iteration were processed by concat to obtain four states Gf, Gi, Go and G, as shown in Fig. 7a. Gf, Gi, and Go are the control signals of forget gate, input gate and output gate, respectively. They were converted to values between 0 and 1 by the sigmoid activation function. G is the input of the neural network input gate, and the result is converted by the tanh activation function. G has a value between −1 and 1. Gf, Gi, Go and G of the current iteration are calculated by the following equations:

$$G(t) = \tanh(W \odot x(t) + W \odot h(t-1)) \quad (1)$$

$$G^f(t) = \sigma\left(W_f \odot x(t) + W_f \odot h(t-1)\right) \quad (2)$$

$$G^i(t) = \sigma(W_i \odot x(t) + W_i \odot h(t-1)) \quad (3)$$

$$G^o(t) = \sigma(W_o \odot x(t) + W_o \odot h(t-1)) \quad (4)$$

Among them, $\odot$ is the Hadamard Product, in which the corresponding elements of the matrix are multiplied. $\oplus$ is matrix addition. W is the weight matrix of the recursive structure in the neural network, and σ represents the sigmoid activation function used in the fully connected layer.

In this study, Bi-LSTM was used as a deep learning model for the prediction of PAP levels. Bi-LSTM is composed of two LSTMs, one is a forward processing sequence and one is a reverse processing sequence (Fig. 7b). The two LSTMs concatenate the processed outputs to get more accurate classification predictions. Compared to LSTM, Bi-LSTM

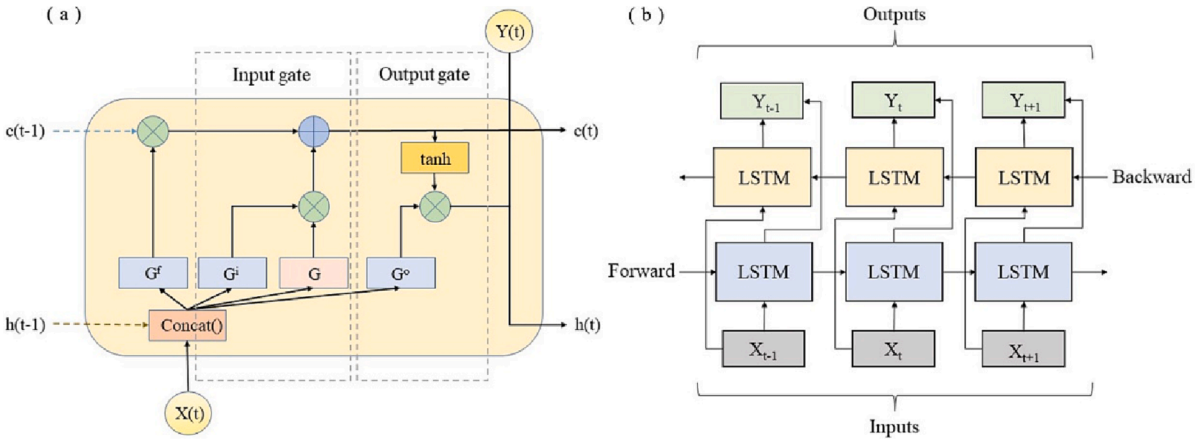

Fig. 7. Architecture of LSTM(a) and Bi-LSTM(b).

network can process temporal data in both forward and backward directions, and has good sequence modeling ability and long short memory ability. It has better performance for 1D signal classification tasks in which time series characteristics were considered [34].The extracted wavelet scattering transform features of PPG signals were input into the Bi-LSTM model.

The dataset was randomly split into 75% training set and 25% test set. The training set was used to train the model and the test set was used to evaluate the performance of the classifier. The model consisted of a 5-layer structure, in which the Bi-LSTM contained 100 hidden units. The training used the Batch and Epoch settings, with a minimum batch size of 1000, and a maximum epoch of 200. The output from the Bi-LSTM network was the predicted PAP levels, specifically, NPP, EPH and PH. The model has been independently trained and tested 5 times as cross validation.

The model was evaluated with several gold standard evaluation parameters: accuracy, sensitivity (true positive rate), specificity (true negative rate), precision (positive predictive value) and F1-score. F1 can evaluate the performance of classification model comprehensively by synthesizing the advantages and disadvantages of precision and sensitivity. These parameters were extracted from the confusion matrix that contains the true positives(TP), true negatives(TN), false positives(FP) and false negatives(FN) for each class. Then the accuracy(Acc), sensitivity(Sen), specificity(Spe), precision(Pre) and F1-score were calculated using the following equations:

$$\mathrm{Acc} = \frac{TP + TN}{TP + TN + FP + FN} \tag{5}$$

$$\mathrm{Sen} = \frac{TP}{TP + FN} \tag{6}$$

$$\mathrm{Spe} = \frac{TN}{TN + FP} \tag{7}$$

$$\mathrm{Pre} = \frac{TP}{TP + FP} \tag{8}$$

$$\mathrm{F1} = \frac{2TP}{2TP + FP + FN} \tag{9}$$

2.5. Experimental methods

Several experiments were designed to optimize or validate the model in this study.

2.5.1. Optimization of signal length

In order to investigate the influence of signal length, an experiment of using signal segments with different length as the model input was designed. The pre-processed PPG signals were cut into 10 s, 30 s and 60 s segments. These signal segments were used as input for the subsequent feature extraction and Bi-LSTM model. In contrast experiment, only the length of input signal segment was different, and other experimental conditions were consistent. Each model was independently trained and tested for 5 times, and the average value for Acc and F1-score were calculated.

2.5.2. Optimization of wavelet scattering transform decomposition framework

In order to explore the effect of the wavelet scattering transform settings on the results, several experiments with only one parameter setting changed each time were conducted. The parameters that can be optimized are InvarianceScale and QualityFactors. InvarianceScale specifies the translational invariance scale of the scattering transform in seconds and defaults to half the signal length. QualityFactors specifies the creation of a wavelet scattering transform network with several filterbanks, with a default of 2 filterbanks. In the optimization, the InvarianceScale was set to 1/2 signal length and 2/3 signal length, respectively. The QualityFactors was set to two filterbanks and three filterbanks respectively. The 30 s signal segment was used for feature extraction and input to the Bi-LSTM model. Each model was independently trained and tested 5 times. The classification accuracy of each experiment was calculated.

2.5.3. CNN, LSTM and Bi-LSTM comparison

The performance of the Bi-LSTM model was compared to conventional models such as CNN and LSTM. The extracted wavelet scattering transform features of PPG signals were input into three models respectively. Pre-processed 30 s signal segment was used for feature extraction. The setting of the wavelet time scattering network was two filterbanks. Each model was independently trained and tested 5 times. Evaluation was performed on all experiments.

3. Results and discussion

3.1. Signal selection and segmentation

In the signal processing section, the dataset was filtered and 34 records with poor PPG signal quality were discarded. 216 recordings were used in the analysis. 90 (41.7%) were labeled as normal pulmonary arterial pressure (NPP), 60 (27.8%) were early pulmonary hypertension (EPH), and the remaining 66 (30.6%) were pulmonary hypertension events (PH). These labels were determined by the value of the pulmonary artery pressure corresponding to each record.

The results of signal length optimization experiment were summarized in Table 2. It can be observed that 30 s and 60 s segments had almost the same performance while 10 s segments were obviously inferior. On the other hand, the computation time for 60 s segments was 50% longer than that of the 30 s segments. Considering both the performance and the computation time, using 30 s window size was the best choice. Therefore, 30 s signal segments were used in all following experiments.

3.2. Results of wavelet time scattering transform network parameter optimization experiment

The results of wavelet time scattering transform network parameter optimization experiment was summarized in Table 3. The accuracy of the wavelet scattering transform framework with three filterbanks was almost the same as that with two filterbanks. The final accuracy of the wavelet scattering transform framework with 1/2 signal length and 2/3 signal length was almost the same. The comparison experiment confirmed that two filterbanks were sufficient to achieve good performance.

3.3. Pulmonary artery pressure states classification and evaluation

PAP classification was performed with the Bi-LSTM method for multiple times and the performance of the model was evaluated. The results were presented in Table4 and Fig. 8.

From the results, the model generally showed satisfactory classification performance, with the mean accuracy of classification of pulmonary arterial pressure in the three states (NPP, EPH and PH) being 99.63%, 98.15% and 97.78%, respectively. Referencing the confusion matrix, it can be seen that the accuracy of NPP is the highest, with

Table 2
Results of the signal length optimization experiment.

Segment	Acc	F1	Time
10 s	93.34%	0.9241	7 s
30 s	97.03%	0.9696	8 s
60 s	97.04%	0.9703	12 s

Table 3
Results of wavelet scattering transform parameter optimization experiment.

InvarianceScale / Acc / QualityFactors	1/2*SignalLength	2/3*SignalLength
[8,1]	97.6%	96.8%
[8,2,1]	96.8%	97.2%

Table 4
Evaluation results of the classification experiments.

N	Class	Acc	Sen	Spe	Pre	F1-socre
1	NPP	98.15%	100%	96.67%	96%	0.9796
	EPH	98.15%	100%	97.5%	93.33%	0.9655
	PH	96.29%	100%	95%	87.5%	0.9333
	NPP	100%	100%	100%	100%	1
	EPH	98.15%	94.44%	100%	100%	0.9714
	PH	98.15%	93.33%	100%	100%	0.9655
	NPP	100%	100%	100%	100%	1
	EPH	98.15%	94.74%	100%	100%	0.9729
	PH	98.15%	93.33%	100%	100%	0.9655
	NPP	100%	100%	100%	100%	1
	EPH	98.15%	90%	100%	100%	0.9474
	PH	98.15%	94.74%	100%	100%	0.973
	NPP	100%	100%	100%	100%	1
	EPH	98.15%	100%	97.56%	92.86%	0.9629
	PH	98.15%	100%	97.5%	93.33%	0.9655
	NPP	99.63%	100%	99.33%	99.2%	0.9959
	EPH	98.15%	95.84%	99.01%	97.24%	0.964
	PH	97.78%	96.28%	98.5%	96.17%	0.9606
Variance	NPP	0.000055	0	0.00018	0.000256	0.00007
	EPH	0	0.001445	0.000147	0.001147	0.00008
	PH	0.000055	0.000949	0.0004	0.002542	0.00019

mostly no error. And there is a higher chance of confusing EPH and PH, especially classifying EPH as PH. This is possibly because sometimes the differentiation between the two states were not as obvious, or when the patient was experiencing a disease state of EPH, approaching PH. In Table 4, the mean and variance of the cross validation experiments were provided. It can be seen that the variance of Acc was 0.000055, which was a reasonable deviation.

The sensitivity and specificity of 95.84% and 99.01% were reported for the prediction of EPH. The sensitivity and specificity of 96.28% and 98.5% were reported for the prediction of PH. The F1-scores of EPH and PH were 0.964 and 0.9606, respectively. Higher F1 scores also indicate better performance of this classification model.

The results of this experiment showed that PPG signal was potentially closely related to pulmonary artery pressure. Pulmonary circulation pressure is controlled by pulmonary blood flow, pulmonary vascular volume, and pulmonary vascular tension [35]. Pathologically, increased pulmonary artery pressure is associated with cardiovascular diseases [36]. As mentioned above, PPG can accurately reflect the state of the cardiovascular circulatory system in real time, which provides a reliable physiological background basis for the relationship between the two. Similarly, the results of the model also verify this relationship.

3.4. Comparison among LSTM, CNN and Bi-LSTM models

To compare the Bi-LSTM model with conventional models, the extracted wavelet scattering transform features of PPG signals were input into the LSTM, CNN, and Bi-LSTM models. The general settings were consistent for all three models. In each experiment, the dataset was randomly split into 75% training set and 25% test set, as was done in previous experiments. The results were summarized in Table 5.

F1m of the LSTM model is 0.9257, while the F1m of CNN model was 0.9365, and F1m of Bi-LSTM is 0.9735. Experimental results showed that the proposed method was superior to CNN and LSTM models in all categories.

Overall, the classification of PAP using PPG signals with the wavelet scattering transform and Bi-LSTM neural network was demonstrated. The parameters were optimized. The model has presented satisfactory results with high accuracy and sensitivity. Compared to conventional deep learning models CNN and LSTM, the proposed method has showed apparently superior results. This method provided an effective tool for evaluating PAP noninvasively and in real time. It is especially useful for continuously monitoring PAP, avoiding pain and risk to patients. Once being demonstrated in much larger dataset, the model can be trained more accurately.

4. Conclusion

In conclusion, in this paper, we have proposed a new method for the classification prediction of pulmonary artery pressure based on PPG signals. A wavelet scattering transform feature extraction method and a Bi-LSTM neural network was adopted. The proposed method showed high accuracy and sensitivity in classifying PAP. This new method showed great promises in identifying pulmonary hypertension events in patients noninvasively and conveniently. In addition, more sophisticated techniques can be developed to extract features from PPG and optimize the deep learning model to improve the performance in PAP

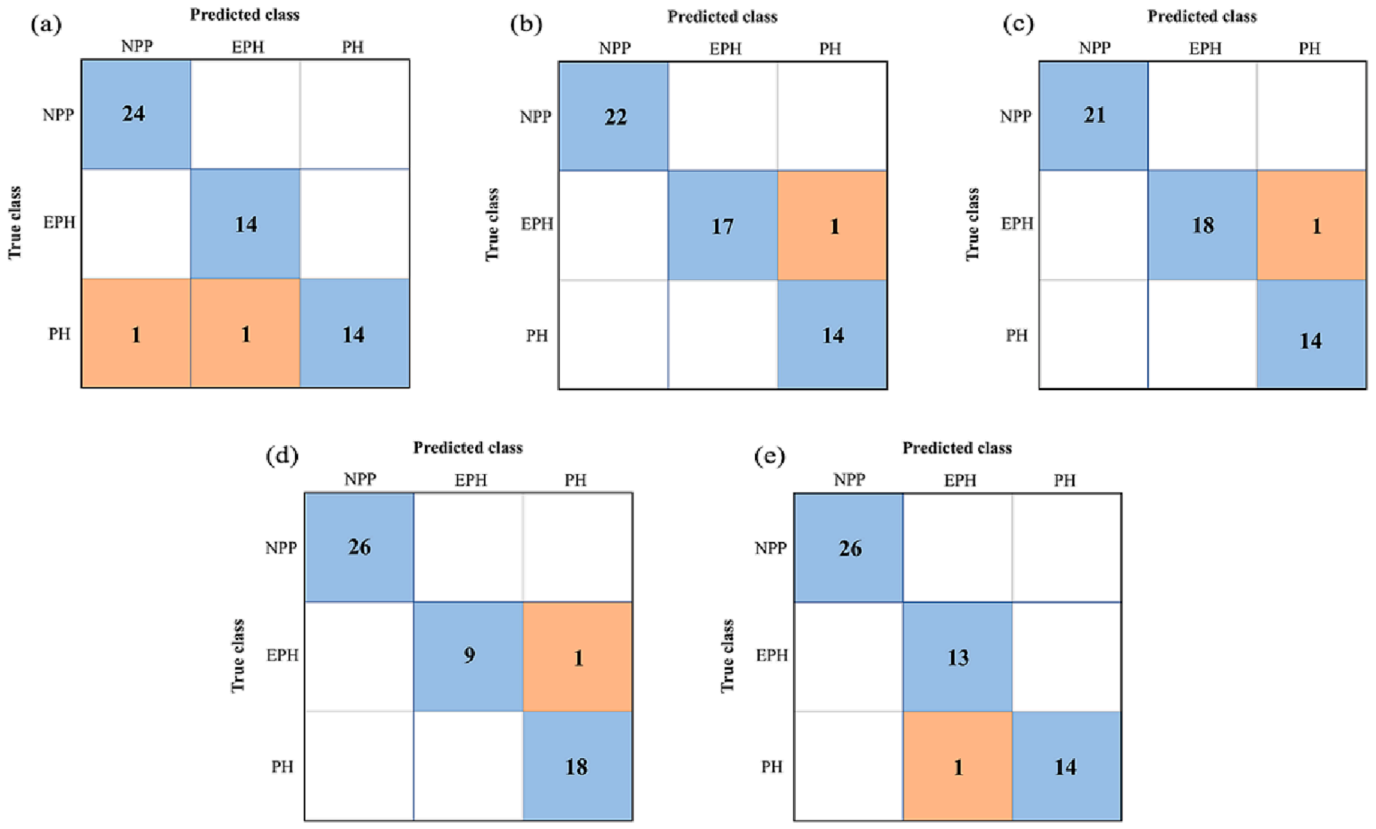

Fig. 8. Confusion matrices of 5 independent training.

Table 5
Comparison of Bi-LSTM with LSTM and CNN.

Model	Class	Pre	Sen	F1	F1m
LSTM	NPP	97.05%	100%	0.9848	0.9257
	EPH	84.94%	93.05%	0.8873	
	PH	87.48%	94.06%	0.9049	
CNN	NPP	96.48%	98.18%	0.9731	0.9365
	EPH	87.99%	98.75%	0.9249	
	PH	88.35%	94.92%	0.9114	
Bi-LSTM	NPP	99.2%	100%	0.9959	0.9735
	EPH	97.24%	95.84%	0.964	
	PH	96.17%	96.28%	0.9606	

prediction, and this may even be combined with other parameters to achieve diagnosis of more complicated diseases. The model will also be combined with wearable devices and enable a noninvasive, continuous, low-cost, convenient-to-use pulmonary hypertension monitoring system to be used in the clinics and homes.

CRediT authorship contribution statement

Qian Zhang: Conceptualization, Methodology, Software, Investigation, Formal analysis, Writing – original draft. **Pei Ma:** Conceptualization, Investigation, Writing – review & editing, Supervision, Project administration.

Declaration of Competing Interest

The authors declare that they have no known competing financial interests or personal relationships that could have appeared to influence the work reported in this paper.

Data availability

Data will be made available on request.

Acknowledgements

The research was financially supported by National Natural Science Foundation of China (No. 62275156, 81700548).

References

[1] M. Obokata, G.C. Kane, H. Sorimachi, Y.N.V. Reddy, T.P. Olson, A.C. Egbe, V. Melenovsky, B.A. Borlaug, Noninvasive evaluation of pulmonary artery pressure during exercise: the importance of right atrial hypertension, Eur. Respir. J. 55 (2020) 1901617, https://doi.org/10.1183/13993003.01617-2019.
[2] G. Simonneau, D. Montani, D.S. Celermajer, C.P. Denton, M.A. Gatzoulis, M. Krowka, P.G. Williams, R. Souza, Haemodynamic definitions and updated clinical classification of pulmonary hypertension, Eur. Respir. J. 53 (2019) 1801913, https://doi.org/10.1183/13993003.01913-2018.
[3] J.J. Ryan, J. Huston, S. Kutty, N.D. Hatton, L. Bowman, L. Tian, J.E. Herr, A. M. Johri, S.L. Archer, Right Ventricular Adaptation and Failure in Pulmonary Arterial Hypertension, Can. J. Cardiol. 31 (2015) 391–406, https://doi.org/10.1016/j.cjca.2015.01.023.
[4] S. Sakao, N. Tanabe, Y. Kasahara, K. Tatsumi, Long-term Survival of Japanese Patients with Pulmonary Arterial Hypertension Treated with Beraprost Sodium, an Oral Prostacyclin Analogue, Intern. Med. 53 (2014) 1913–1920, https://doi.org/10.2169/internalmedicine.53.2573.
[5] D.B. Badesch, H.C. Champion, M.A. Gomez Sanchez, M.M. Hoeper, J.E. Loyd, A. Manes, M. McGoon, R. Naeije, H. Olschewski, R.J. Oudiz, A. Torbicki, Diagnosis and Assessment of Pulmonary Arterial Hypertension, J. Am. College Cardiol. 54 (2009) S55–S66, https://doi.org/10.1016/j.jacc.2009.04.011.
[6] M. D'Alto, K. Dimopoulos, J.G. Coghlan, G. Kovacs, S. Rosenkranz, R. Naeije, Right Heart Catheterization for the Diagnosis of Pulmonary Hypertension, Heart Failure Clinics. 14 (2018) 467–477, https://doi.org/10.1016/j.hfc.2018.03.011.
[7] S. Rosenkranz, I.R. Preston, Right heart catheterisation: best practice and pitfalls in pulmonary hypertension, Eur. Respir. Rev. 24 (2015) 642–652, https://doi.org/10.1183/16000617.0062-2015.
[8] S. Shah, G. Boyd, C.T. Pyne, S.D. Bilazarian, T.C. Piemonte, C. Jeon, S. Waxman, Right heart catheterization using antecubital venous access: Feasibility, safety and

adoption rate in a tertiary center, Cathet. Cardiovasc. Intervent. 84 (2014) 70–74, https://doi.org/10.1002/ccd.25249.
[9] M.V. Di Maria, D.A. Burkett, A.K. Younoszai, B.F. Landeck, L. Mertens, D.D. Ivy, M. K. Friedberg, K.S. Hunter, Echocardiographic Estimation of Right Ventricular Stroke Work in Children with Pulmonary Arterial Hypertension: Comparison with Invasive Measurements, J. Am. Soc. Echocardiogr. 28 (2015) 1350–1357, https://doi.org/10.1016/j.echo.2015.07.017.
[10] Y. Li, Y. Wang, H. Li, W. Zhu, X. Meng, X. Lu, Evaluation of the hemodynamics and right ventricular function in pulmonary hypertension by echocardiography compared with right-sided heart catheterization, Exper. Therapeutic Med. 14 (2017) 3616–3622, https://doi.org/10.3892/etm.2017.4953.
[11] R. Naeije, M. D'Alto, P.R. Forfia, Clinical and Research Measurement Techniques of the Pulmonary Circulation: The Present and the Future, Progr. Cardiovasc. Dis. 57 (2015) 463–472, https://doi.org/10.1016/j.pcad.2014.12.003.
[12] A.A. Alian, K.H. Shelley, Photoplethysmography, Best Pract. Res. Clin. Anaesthesiol. 28 (2014) 395–406, https://doi.org/10.1016/j.bpa.2014.08.006.
[13] V. Rybynok, J.M. May, K. Budidha, P.A. Kyriacou, Design and development of a novel multi-channel photoplethysmographic research system, in: 2013 IEEE Point-of-Care Healthcare Technologies (PHT), IEEE, Bangalore, India, 2013: pp. 267–270. https://doi.org/10.1109/PHT.2013.6461336.
[14] M. Elgendi, R. Fletcher, Y. Liang, N. Howard, N.H. Lovell, D. Abbott, K. Lim, R. Ward, The use of photoplethysmography for assessing hypertension, Npj Digit. Med. 2 (2019) 60, https://doi.org/10.1038/s41746-019-0136-7.
[15] J. Allen, D. Zheng, P.A. Kyriacou, M. Elgendi, Photoplethysmography (PPG): state-of-the-art methods and applications, Physiol. Meas. 42 (2021) 100301, https://doi.org/10.1088/1361-6579/ac2d82.
[16] Y. Tabara, M. Igase, Y. Okada, T. Nagai, T. Miki, Y. Ohyagi, F. Matsuda, K. Kohara, Usefulness of the second derivative of the finger photoplethysmogram for assessment of end-organ damage: the J-SHIPP study, Hypertens Res. 39 (2016) 552–556, https://doi.org/10.1038/hr.2016.18.
[17] E. Mejía-Mejía, J.M. May, M. Elgendi, P.A. Kyriacou, Classification of blood pressure in critically ill patients using photoplethysmography and machine learning, Comput. Methods Programs Biomed. 208 (2021) 106222, https://doi.org/10.1016/j.cmpb.2021.106222.
[18] E.M. Green, R. van Mourik, C. Wolfus, S.B. Heitner, O. Dur, M.J. Semigran, Machine learning detection of obstructive hypertrophic cardiomyopathy using a wearable biosensor, Npj Digit. Med. 2 (2019) 57, https://doi.org/10.1038/s41746-019-0130-0.
[19] Z.S. Hosseini, E. Zahedi, H. Movahedian Attar, H. Fakhrzadeh, M.H. Parsafar, Discrimination between different degrees of coronary artery disease using time-domain features of the finger photoplethysmogram in response to reactive hyperemia, Biomed. Signal Process. Control. 18 (2015) 282–292, https://doi.org/10.1016/j.bspc.2014.12.011.
[20] J. Allen, Photoplethysmography and its application in clinical physiological measurement, Physiol. Meas. 28 (2007) R1–R39, https://doi.org/10.1088/0967-3334/28/3/R01.
[21] Y. Liang, Z. Chen, R. Ward, M. Elgendi, Hypertension Assessment Using Photoplethysmography: A Risk Stratification Approach, JCM. 8 (2018) 12, https://doi.org/10.3390/jcm8010012.
[22] S.-K. Lin, H. Hsiu, H.-S. Chen, C.-J. Yang, Classification of patients with Alzheimer's disease using the arterial pulse spectrum and a multilayer-perceptron analysis, Sci. Rep. 11 (2021) 8882, https://doi.org/10.1038/s41598-021-87903-7.
[23] M. Radha, P. Fonseca, A. Moreau, M. Ross, A. Cerny, P. Anderer, X. Long, R. M. Aarts, A deep transfer learning approach for wearable sleep stage classification with photoplethysmography, Npj Digit. Med. 4 (2021) 135, https://doi.org/10.1038/s41746-021-00510-8.
[24] A.L. Goldberger, L.A.N. Amaral, L. Glass, J.M. Hausdorff, P.C. Ivanov, R.G. Mark, J. E. Mietus, G.B. Moody, C.-K. Peng, H.E. Stanley, PhysioBank, PhysioToolkit, and PhysioNet: Components of a New Research Resource for Complex Physiologic Signals, Circulation. 101 (2000), https://doi.org/10.1161/01.CIR.101.23.e215.
[25] A.E.W. Johnson, T.J. Pollard, L. Shen, L.H. Lehman, M. Feng, M. Ghassemi, B. Moody, P. Szolovits, L. Anthony Celi, R.G. Mark, MIMIC-III, a freely accessible critical care database, Sci. Data. 3 (2016) 160035, https://doi.org/10.1038/sdata.2016.35.
[26] C.K. Chui, An introduction to wavelets, Academic Press, Boston, 1992.
[27] S. Mallat, Group Invariant Scattering, Comm. Pure Appl. Math. 65 (2012) 1331–1398, https://doi.org/10.1002/cpa.21413.
[28] Y.-L. Boureau, F. Bach, Y. LeCun, J. Ponce, Learning mid-level features for recognition, in: 2010 IEEE Computer Society Conference on Computer Vision and Pattern Recognition, IEEE, San Francisco, CA, USA, 2010: pp. 2559–2566. https://doi.org/10.1109/CVPR.2010.5539963.
[29] J. Bruna, S. Mallat, Invariant Scattering Convolution Networks, IEEE Trans. Pattern Anal. Mach. Intell. 35 (2013) 1872–1886, https://doi.org/10.1109/TPAMI.2012.230.
[30] Y. Yu, X. Si, C. Hu, J. Zhang, A Review of Recurrent Neural Networks: LSTM Cells and Network Architectures, Neural Comput. 31 (2019) 1235–1270, https://doi.org/10.1162/neco_a_01199.
[31] A. Sherstinsky, Fundamentals of Recurrent Neural Network (RNN) and Long Short-Term Memory (LSTM) network, Physica D: Nonlinear Phenomena 404 (2020) 132306, https://doi.org/10.1016/j.physd.2019.132306.
[32] X. Qing, Y. Niu, Hourly day-ahead solar irradiance prediction using weather forecasts by LSTM, Energy. 148 (2018) 461–468, https://doi.org/10.1016/j.energy.2018.01.177.
[33] F.A. Gers, E. Schmidhuber, LSTM recurrent networks learn simple context-free and context-sensitive languages, IEEE Trans. Neural Netw. 12 (2001) 1333–1340, https://doi.org/10.1109/72.963769.
[34] Z. Huang, W. Xu, K. Yu, Bidirectional LSTM-CRF Models for Sequence Tagging, (2015). http://arxiv.org/abs/1508.01991 (accessed April 14, 2023).
[35] Y.-C. Lai, K.C. Potoka, H.C. Champion, A.L. Mora, M.T. Gladwin, Pulmonary Arterial Hypertension: The Clinical Syndrome, Circ. Res. 115 (2014) 115–130, https://doi.org/10.1161/CIRCRESAHA.115.301146.
[36] M. Brida, M.A. Gatzoulis, Pulmonary arterial hypertension in adult congenital heart disease, Heart. 104 (2018) 1568–1574, https://doi.org/10.1136/heartjnl-2017-312106.